Tellus (1992), *44A*, 54–66

Geostrophic drag coefficients over sea ice

By JAMES E. OVERLAND, *Pacific Marine Environmental Laboratory, National Oceanic and Atmospheric Administration*, 7600 Sand Point Way NE, Seattle, WA 98115-0070, USA*, and KENNETH L. DAVIDSON, *Naval Postgraduate School, Monterey, CA 93943-5000, USA*

(Manuscript received 11 October 1990; in final form 5 March 1991)

ABSTRACT

The geostrophic drag coefficient, $C_g \equiv u_*/G$, and turning angle, α, were measured October through November 1988 from a 120 km array of 6 drifting buoys and a drifting ship in the northern Barents Sea/Arctic Ocean during CEAREX; u_* is the friction velocity, G is the geostrophic wind, and α is the angle between surface stress and $\vec{G}$. The median Cg was 0.029 with hinge values (quartiles) of 0.023 and 0.034 and the median α was 25° with hinge values of 15° and 32°. The median values are representative for the non-summer Arctic away from marginal seas and marginal ice zones. Surface air temperature, cloud amount, and the lapse rate above the inversion base were not good predictors of the influence of boundary layer stability on Cg. The geostrophic drag coefficient was most sensitive to the temperature difference across the boundary layer from the surface to the top of the inversion. A first order correction to account for airmass stability is

$$Cg = 0.037 - 8.3 \times 10^{-3} \left(\frac{N_{900}}{\bar{N}_{900}}\right)^4, \qquad \alpha = 11.7 + 13.1 \left(\frac{N_{900}}{\bar{N}_{900}}\right)^2.$$

This stability correction represents a 17% improvement over using a constant drag value, based on reduction of variance with the CEAREX data set. The formula uses an external stability parameter, N^2_{900}, proportional to the difference between the potential temperature measured at 900 mb, θ_{900}, which is representative of the temperature at the top of the arctic inversion, and at the surface, θ_s: $N^2_{900} = (g/\bar{\theta})\,\Delta\theta/h_{900}$, $\Delta\theta = \theta_{900} - \theta_s$, $\bar{\theta} = (\theta_{900} + \theta_s)/2$, $h_{900} = 67.4\bar{\theta}\log_{10}(P_s/900)$, $\bar{N}_{900} = 0.024\ \mathrm{s}^{-1}$, P_s is surface pressure and g is gravity. θ_{900} can be obtained from atmospheric models or satellite-derived temperature soundings. Formulas are also developed based on the standard level of 850 mb; the reduction in variance is less, 11%, because this level is sometimes above the top of the arctic inversion. We reason that because most of the boundary layer above the surface layer is near a critical Richardson number, the total amount of shear that can be maintained in the boundary layer, and thus the reduction in Cg, is given by the external temperature difference rather than the detailed internal structure of stratification and shear. Corrections are also proposed for change in surface roughness. Although the thermal wind was estimated from the buoy array and is important for case studies, it did not provide significant improvement in reducing the variability in the geostrophic drag measurements.

1. Introduction

Winds are the primary driving force for ice motion in most regions of the Arctic (Thorndike and Colony, 1982) and probably the Antarctic. An objective of high-latitude meteorology is to relate air/ice/ocean exchange of momentum and heat to basic atmospheric variables, such as geostrophic wind, or to atmospheric-model derived wind fields for use in driving sea-ice models (Hibler and Walsh, 1982; Preller and Posey, 1989). The principal parameter is the geostrophic drag coefficient, Cg, and the cross-isobaric or turning angle, α

$$Cg \equiv u_*/G \tag{1}$$

$$u_*^2 \equiv \tau/\rho \tag{2}$$

$$\alpha \equiv \text{angle between } \vec{\tau} \text{ and } \vec{G} \tag{3}$$

* Contribution No. 1223 from NOAA/Pacific Marine Environmental Laboratory

where u_* is a friction velocity, $\vec{\tau}$ is the regional air-ice stress, ρ is air density and $\vec{G}$ is either the geostrophic or gradient wind, derived from the sea-level pressure field.

If Cg and α were constants, the issue of atmospheric forcing would be straightforward. However, individual measurements of these parameters show variability due to their sensitivity to heterogeneous surface roughness, atmospheric boundary layer (ABL) processes and measurement difficulties (Fiedler and Panofsky, 1972; Overland, 1985). Modeling studies show the geostrophic drag coefficient is 25% smaller during cases of strong surface stability or low atmospheric temperature inversions than in well-mixed boundary layers, and turning angles can be 15° greater during stable conditions (Brown, 1981). A second source of variability is that the geostrophic wind is not always the local forcing of the ABL. If there is curvature to the sea-level pressure field such as flow around a low pressure center, the gradient wind rather than the geostrophic wind is appropriate. The gradient wind can be 20% smaller than the geostrophic wind for low-pressure weather systems. If the sea-level pressure field is provided on a regular grid, the gradient wind can be calculated with standard formulas (Appendix; Overland et al., 1980). If there are horizontal temperature gradients in the region, as is often the case near the polar front in the Arctic, these gradients imply that the geostrophic wind varies with height, i.e., the thermal wind. ABL forcing is the result of the average geostrophic wind throughout the boundary layer, not simply the surface geostrophic wind derived from the sea-level pressure gradient (Carsey and Leavitt, 1977; Danard, 1988). The ability to relate Cg and α to atmospheric variables through similarity theory based only on surface buoyancy flux and rotation has not been very successful in accounting for the variability in observations of the mechanically mixed ABL, such as the winter Arctic (Kitaigorodskii, 1988).

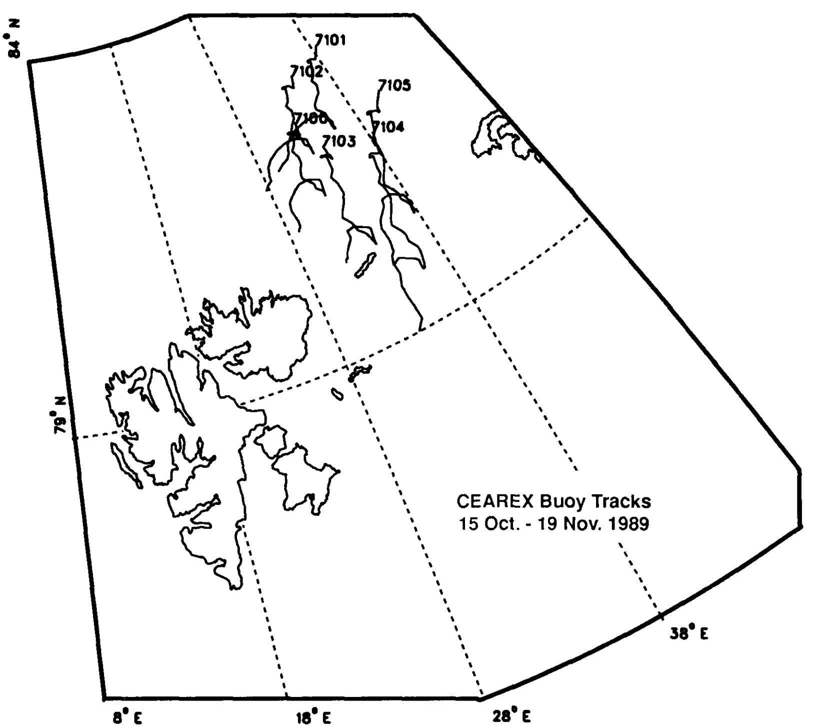

Fig. 1. Location map for the CEAREX drift. The tracks of the six ARGOS drifters are shown from 15 October to 19 November 1988.

From September through December 1988 measurements of geostrophic wind and thermal wind were made north and east of Svalbard in the northern Barents Sea from an array of six drifting ARGOS buoys (Fig. 1). This array was centered on the *Polarbjorn*, a research vessel drifting with the ice, which collected surface meteorological data and atmospheric profile data from weather balloon launches as part of the Coordinated Eastern Arctic Experiment (CEAREX Drift Group, 1990). The purpose of this paper is to provide an estimate of the geostrophic drag coefficient and turning angle for the region of small to medium, rough multiyear floes, characteristic of the eastern Arctic. We then investigate possible refinement of these values based on ABL stability, inversion structure and thermal wind. We investigate whether routinely available information such as cloud amount or temperature profiles obtained from satellite or routine analyses at standard levels and atmospheric model output can be used to improve estimates of geostrophic drag.

2. Conceptual model of the Arctic ABL

We are principally concerned with the eight month winter season, October through May, when solar heating makes a negligible contribution to the total surface arctic radiation budget. Typical winter temperature soundings are shown in Fig. 2. The sounding is characterized by a temperature maximum layer between 950–850 mb which is maintained by a balance between horizontal heat advection from lower latitudes and radiative cooling (Overland and Guest, 1991). During quiescent periods this layer tends to become isothermal due to radiative transfer (Fig. 2a). Below this layer is the arctic inversion in which air temperature increases with height. The temperature profile may show a surface-based inversion as in Fig. 2b or have a less stable layer next to the surface and an elevated inversion base during the presence of surface-layer mixing. Snow temperature depends strongly on the surface radiation balance and in particular the downward component of longwave radiation; given clear sky conditions, the surface temperature is relatively cold. *An external measure of the stability of the arctic ABL is thus given by the potential temperature difference between the temperature maximum layer and the snow-surface temperature.* We expect northerly winds, cold air temperatures, clear skies and low inversions to correlate with each other and with small Cg and large α (Walter and Overland, 1991). During cloudy conditions, often with warm air advection from the south, the snow temperature increases and the surface-layer

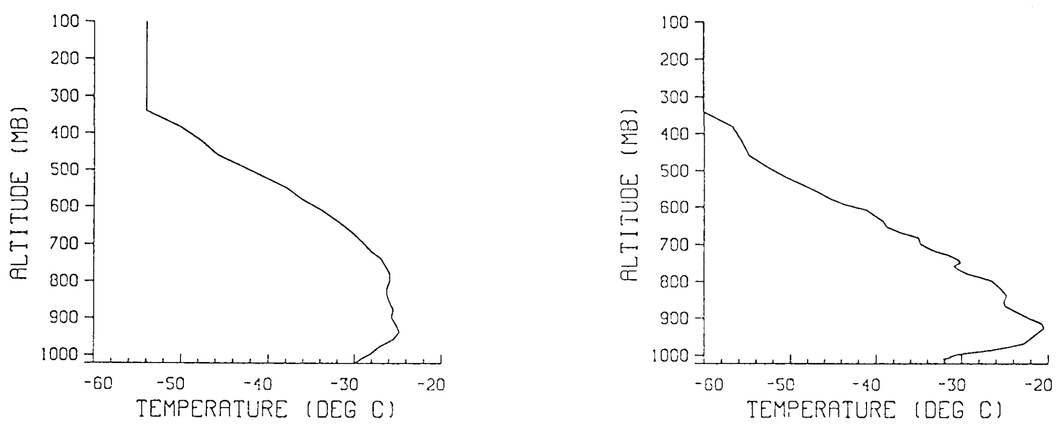

Fig. 2. Typical winter temperature sounding for the CEAREX site, 4 November 1988 and 27 November 1988. There is a temperature maximum layer near 850–950 mb with a more adiabatic lapse rate above. Below the temperature maximum is a layer of strong stratification, the inversion layer. This stratification can extend to the surface during light winds or there may be a shallow slightly stable layer next to the surface forming an inversion base at the temperature discontinuity.

thickness increases; one expects better air-ice coupling with greater Cg and smaller α.

It is well known that the height of the inversion base rises with increasing wind speed (Sverdrup, 1933), i.e., increasing turbulent kinetic energy and increased u_*. Our conceptual model is that radiative cooling at the snow surface and maintenance of the temperature maximum layer through horizontal advection establish the ABL stratification, and that mechanical mixing by increasing wind speeds establishes the height of the inversion base. One approach to remove wind speed dependence is to scale the actual inversion base height, Z_i, by the height of the ABL without thermal forcing, i.e., only mechanical mixing

$$Z_*^{-1} = \frac{Z_i}{L_E}, \qquad L_E = u_*/f. \tag{4}$$

The primary variations in L_E is considered to be from u_* and not the Coriolis parameter, f. From numerical studies based on a turbulent closure ABL model, large Z_*, i.e., small Z_i relative to L_E, shows small Cg and large α (Fig. 3; Overland, 1985).

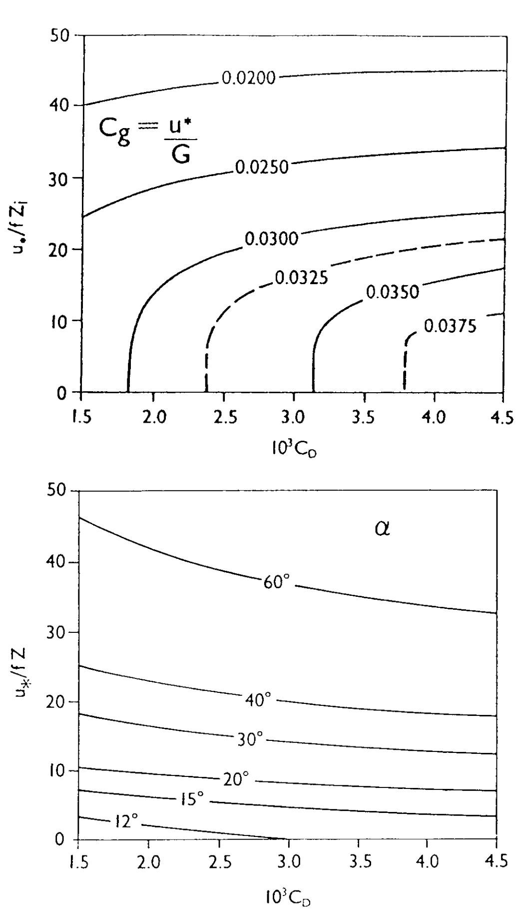

Fig. 3. Model results of the dependence of Cg and α on normalized inversion height, Z_*^{-1}, and surface roughness as measured by the 10 m drag coefficient, C_D (Overland, 1985). Low inversions are characteristic of Z_* values greater than 20 with greater α and smaller Cg. The importance of surface roughness on Cg is reduced for greater values of Z_*.

Kitaigorodskii and Joffre (1988) state that the structure of the stable ABL such as the Arctic should relate to the background stratification, i.e., inversion strength, in addition to the two parameters of classical Kazanski-Monin similarity theory: surface buoyancy and rotation. They argue that the inversion height in cases like the arctic ABL where mechanical mixing is important should scale as the ratio of turbulent kinetic energy production to the ABL stratification

$$L_N = u_*/N \tag{5}$$

where N is the Väisälä frequency for the lapse rate of the stable layer above the inversion base

$$N^2 = \frac{g}{\theta}\frac{d\theta}{dz}, \tag{6}$$

g is gravity and θ is potential temperature. Note both (4) and (5) consider stability of the ABL and are not related to surface layer similarity, Obukhov length, etc., based on air-snow buoyancy fluxes, which are small (Overland and Guest, 1991).

3. The data set

The data were divided into three subsets. The first subset (A) is 817 hourly values of geostrophic wind and horizontal temperature gradient from an array of six drifting ARGOS buoys, combined with hourly values of wind and temperature at the ship. The buoy data was fit by second-order splines and resampled. The buoys were originally placed 60 km from the *Polarbjorn*; with time the array became elongated in a north-south direction (Fig. 1). We begin all the data sets on 15 October

1988 after winter-type conditions (-19°C air temperatures) were established. Data set A continues to 19 November when the buoy array was considered too deformed for reliable estimates of geostrophic wind. The second subset (B) consists of 121 12-hourly values collected by weather balloon from the drifting ship from 16 October to 31 December 1988. This data includes surface winds, air temperature, cloud amounts, inversion height, inversion thickness and inversion strength. Subset C is the intersection of data sets A and B.

The ship drifted generally south and was at 82.1° N 36.9° E on 16 October, 80.4° N 31.5° E on 19 November and 76.6° N 28.0° E on 31 December. Winds and air temperature were measured on a bow mast at a height of 14 m (U_{14}); winds have been adjusted to 10 m (U_{10}) with a constant factor of 0.95. Vertical profiles of temperature were obtained through a rawinsonde system. The inversion base height was calculated as the lowest discontinuity in the temperature profile. Although the system measures winds via Omega tracking these winds are not valid for the ABL due to lack of vertical resolution. A 6 m profile mast was installed on the ice which measured temperature and wind speeds at 4 levels to make estimates of the surface drag coefficient and heat flux. The snow temperature measured by a thermistor at the base of the profile mast was generally within one degree of the air temperature at 6 m (Overland and Guest, 1991). In further analyses the surface air temperature from the bow mast is used.

For this paper estimates of u_* are made from the ship anemometer

$$u_* \equiv C_{\mathrm{Do}}^{1/2} U_{10}, \tag{7}$$

where C_{Do} is the regional 10 m neutral drag coefficient for the CEAREX region. Based on the profile mast, P. Guest (personal communication) has estimated a C_{D} for the floe in the vicinity of the *Polarbjorn* as 2.3×10^{-3} for the period before 17 November; during this time ice conditions did not vary and the ice roughness was constant. After this data floes started breaking up and the measured drags were $C_{\mathrm{D}} > 3.3 \times 10^{-3}$. Regional roughness is in general greater than that measured from masts mounted on the smooth part of floes (Joffre, 1983; Overland, 1985). We adopt a value $C_{\mathrm{Do}} = 2.5 \times 10^{-3}$ for the period before 19 November consistent with visual estimates of regional roughness (Guest and Davidson, 1987) and consistent with the tower estimate. This value of C_{Do} is a typical regional value for winter arctic pack ice (Overland, 1985).

4. Results

Table 1 presents the median and hinge values for Cg, α, and U_{14}/G for data set A. Medians are used instead of means because they are less sensitive to outlier data points. Hinges are the values for which one quarter of the data are greater or less. The width of the center of distributions between the hinge values are rather narrow and the tails are broad (Fig. 4). For the large data set we plot Cg versus geostrophic wind direction (Fig. 5), which may correlate with arctic versus more maritime air masses. There is a significant difference at the 95% confidence level (Snedecor and Cochran, 1989) in Cg and α (Table 2) between air trajectories from southerly wind directions (90° to 270°) compared to northerly (270° to 90°). To consider the influence of stratification it is tempting to plot Cg versus L_N; however, this is not a valid approach because u_* appears in the numerator of both expressions. A plot of Cg versus stratification based on surface air temperature, θ_s, only

$$N_s^2 = \frac{g}{\theta_s} \frac{(263° - \theta_s)}{100\ \mathrm{m}} \tag{8}$$

provides no strong correlation (Fig. 6). The value of 263° is taken as a typical value for the temperature maximum layer and thus N_S was proposed as an external stability parameter for the ABL.

Table 1. *Values of geostrophic drag coefficient, Cg, inflow angle between the surface and geostrophic wind, α, and the ratio of ship wind speed to geostrophic wind speed for the 15 October–19 November CEAREX drift phase north of Svalbard*

	Lower hinge	Median	upper hinge
Cg	0.023	0.029	0.034
α	15.0	24.5	31.7
U_{14}/G	0.47	0.58	0.69

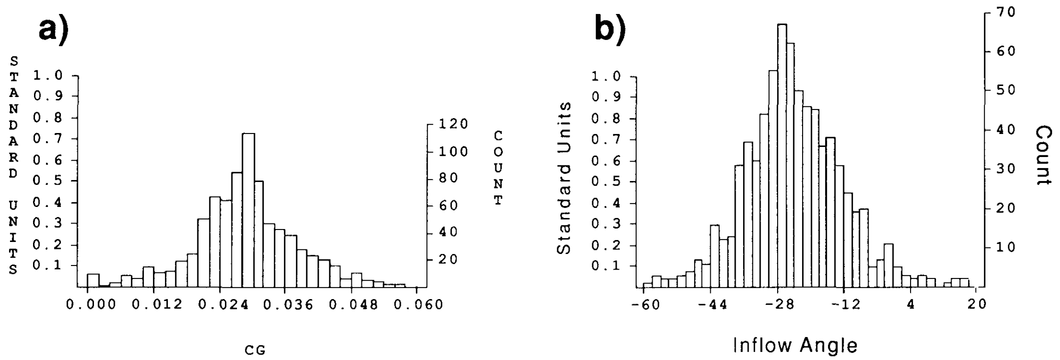

Fig. 4. (a) Distribution of geostrophic drag coefficient, $Cg = u_*/G$, as measured northeast of Svalbard during the fall 1988 CEAREX drift. (b) Distribution of inflow angle between the surface and geostrophic wind for the CEAREX drift.

We can replace $\vec{G}$ with a layer average geostrophic wind

$$\vec{G}_{\mathrm{T}} = \vec{G} - \frac{gH_i}{2f\theta_s} \nabla \times \theta_s, \tag{9}$$

where H_i is taken as 200 m. We find no significant reduction in variance of Cg or α with replacing $\vec{G}$ by $\vec{G}_{\mathrm{T}}$ (Table 3). It is known that the thermal wind can be very important to the value of Cg and α in individual case studies of cold air advection (Walter et al., 1984); however, if there is any dependence on thermal wind in data set A it is masked by the overall variability.

We conclude that there is a dependence of Cg and α on air mass in the CEAREX data set A and that further investigation is required of the other data sets. We next bin the observations in data set C for southerly and northerly wind components (Table 4). We include Cg, α, Z_i, Z_*, total cloud (0–8), θ_s and stability measures L'_N, L_{500},

$$L'_N = u_*/N', \qquad N' = \left(\frac{g}{\theta_s} \frac{\Delta\theta'}{(Z_{\mathrm{TOP}} - Z_i)}\right)^{1/2} \tag{10}$$

$$L_{500} = u_*/N_{500}, \qquad N_{500} = \left(\frac{g}{\bar{\theta}_{500}} \frac{\Delta\theta_{500}}{500\ \mathrm{m}}\right)^{1/2},$$

$$\bar{\theta}_{500} = (\theta_{500} + \theta_{\mathrm{S}})/2, \qquad \Delta\theta_{500} = \theta_{500} - \theta_{\mathrm{S}}, \tag{11}$$

where Z_{TOP} is the next significant temperature discontinuity above Z_i and $\Delta\theta'$ is the temperature difference between Z_{TOP} and Z_i, θ_{500} is the potential temperature at 500 m. N' represents the observed

Table 2. *Values of geostrophic drag and inflow angle for southerly (90° to 270°) and northerly (270° to 90°) geostrophic wind directions. The medians of the geostrophic drag are significantly different from each other at the 95% confidence level*

		Low hinge	Median	Upper hinge
southerly (615 cases)	Cg	0.025	0.030	0.035
	α	14.8	23.9	29.7
northerly (202 cases)	Cg	0.015	0.024	0.029
	α	15.9	27.8	38.7

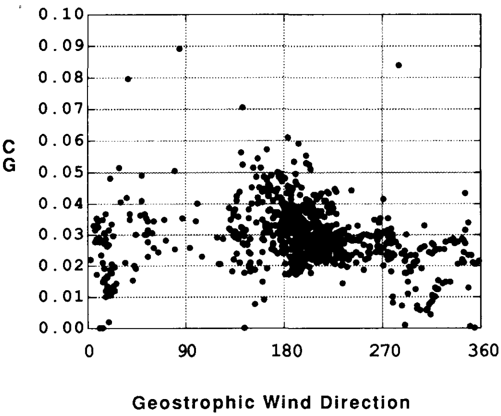

Fig. 5. Plot of Cg versus direction of the geostrophic wind. There are more values of $Cg < 0.02$ for directions $< 90°$ and $> 270°$ than for wind directions of 90° to 270°.

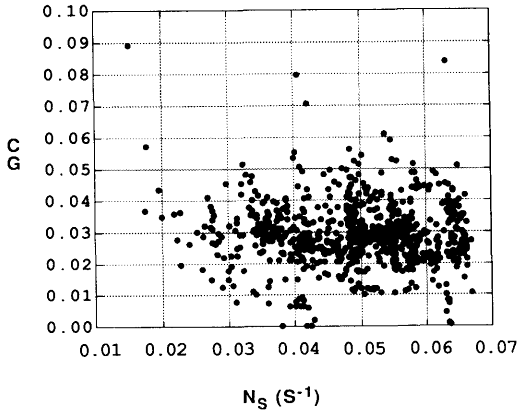

Fig. 6. Plot of *Cg* versus surface temperature normalized by the Brunt-Väisälä frequency $N_s^2 = (g/\theta_s)(263° - \theta_s)/100$ m. There is no strong visual correlation.

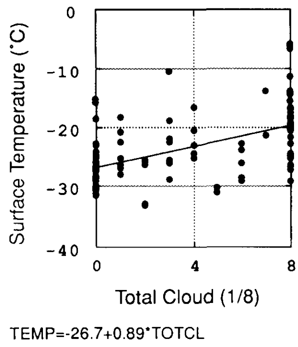

Fig. 7. Plot of cloud versus surface temperature for the entire CEAREX period (Data set B).

stratification in the inversion layer and N_{500} represents an external stratification parameter for the ABL based on an upper air temperature and the surface air temperature. Recall N_s was a stability measure based only on surface air temperature in contrast to N_{500}. The difference in *Cg* and α in Table 4 reflect the same differences as in the larger data set. Z_i are lower for northerly winds. There is a good separation in Z_* between northerly and southerly winds, and smaller *Cg* is associated with $Z_* > 20$. Seventy percent of the southerly wind data have $Z_* < 20$. Northerly winds also have lower values of L_{500} (stronger normalized ABL stratification) than southerly winds, although there is little directional difference

Table 3. *Statistics for Cg and inflow angle for inclusion of the thermal wind*

	Lower hinge	Median	Upper hinge
Cg	0.024	0.029	0.035
α	14.5	23.3	30.6

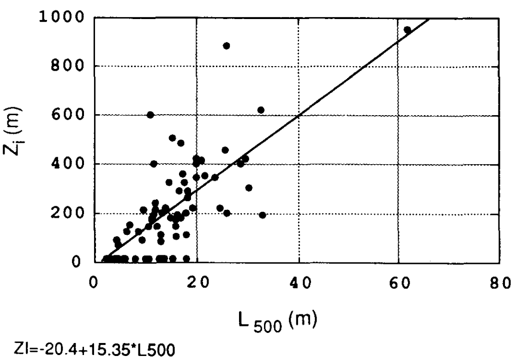

Fig. 8. Plot of observed inversion base height versus stability length $L_{500} = u_*/N_{500}$.

Table 4. *Medians and quantiles for geostrophic wind direction from the south and from the north*

	Northerly wind (14 cases)			Southerly wind (56 cases)		
Variable	Lower hinge	Median	Upper hinge	Lower hinge	Median	Upper hinge
Cg	0.015	0.024	0.030	0.025	0.029	0.038
α	13.3	26.3	36.6	12.0	21.6	27.5
Z_i (m)	0	130	200	105	205	380
Z_*	11.2	22.2	62.6	8.2	13.4	24.4
θ_s	−24.4	−19.1	−17.0	−26.4	−24.6	−21.0
L'_N (m)	5.55	8.34	11.56	6.05	8.96	11.92
L_{500} (m)	5.73	11.19	17.62	11.67	15.59	19.76
cloud amount	4	8	8	0	1	7

related to L'_N. Warmer surface values correlate with increasing clouds as expected; contrary to intuition, these occur with northerly winds. From data set B we also find that warmer surface temperatures occur with overcast conditions (Fig. 7); an expected result (Overland and Guest, 1991). As proposed by Kitaigorodskii and Joffre (1988) the stability length L_{500} is a good predictor of inversion height ($R = 0.72$, data set B)

$$Z'_i = -20.4 + 15.3 L_{500}. \tag{12}$$

The negative intercept accounts for surface based inversions while L_{500} remains finite (Fig. 8).

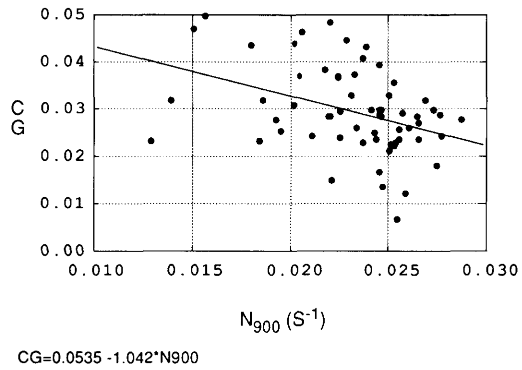

Fig. 9. Plot of *Cg* versus N_{900}. A regression curve is also plotted.

5. Discussion

Decreasing geostrophic drag coefficients and increasing turning angle do correlate with northerly wind direction, lower normalized inversions, and stronger ABL stratification, as measured by the external stability parameter, L_{500}. Surface air temperature by itself is not a good surrogate measure of ABL stratification. Increasing cloud amount correlates with warmer surface temperatures as expected from the increase in downward longwave radiation. Therefore, we conclude that the ABL stratification is determined by the air temperature above the surface layer as much as by the surface temperature. The air temperature in the temperature maximum layer is maintained by advection from more southerly latitudes (Overland and Guest, 1991). Synoptic activity was certainly present while the *Polarbjorn* was north of 81°N and is ubiquitous in the Arctic (Serreze and Barry, 1988). The presence of clouds with northerly winds may be due to the passage of cyclonic weather systems to the south and east of the *Polarbjorn* location during fall 1988. The main points of Kitaigorodskii and Joffre (1988) are confirmed: that the external ABL stratification is important to specifying the structure of the ABL and not simply surface layer fluxes. In addition, the difference between an upper level and surface temperature was a better predictor of ABL variability than the stability measured internally in the ABL above the inversion base, N', probably due to measurement variability in N' or that velocity shear is important throughout the ABL rather than just above the inversion base.

The range of *Cg* for upper and lower hinges for the complete data set (Table A) are 0.023 to 0.034 or about 20% of the median value. This range is consistent with winter Arctic values of *Cg* obtained during AIDJEX from aircraft measurements (Katz, 1979) of 0.025 (stable stratification), 0.032

Table 5. *Correlation coefficient of geostrophic drag and turning angle with one internal, N', and three external stratification parameters; the number of data points is 61*

	N'	N_{500}	N_{900}	N_{850}
Cg	0.02	0.17	0.39	0.33
α	0.02	0.35	0.30	0.31

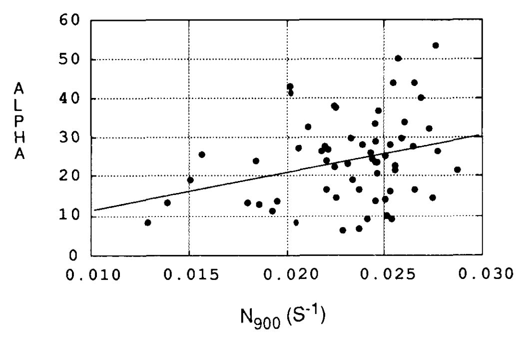

Fig. 10. Plot of α versus N_{900}. A regression curve is also plotted.

(near neutral stratification) and from momentum integral techniques of 0.026–0.028 (Carsey and Leavitt, 1977). Because there is good comparison between CEAREX and AIDJEX observations, we can recommend values of $Cg = 0.028$ and $\alpha = 25°$ for use in modeling ice drift in the central Arctic during the winter season, October through May; here we have averaged the Carsey and Leavitt value with our CEAREX median value. Evidence of Thorndike and Colony (1982) from ice velocity-geostrophic wind ratios also supports our conclusion of no major geographic variation of Cg in the central Arctic.

Because the regional surface roughness was constant during the CEAREX measurement period, we assume that the observed variability during CEAREX is due primarily to ABL stratification. By using expressions (4) and (12) we form the normalized stratification value

$$Z'_* = \frac{L_E}{Z'_i} \sim \frac{L_E}{L_N} = \frac{N}{f}. \tag{13}$$

We argue that the ratio in (13) is an appropriate non-dimensional scaling for Cg because if the length scale for stratification, L_N, is greater than for the neutral case, L_E, then the ABL would resemble the neutral case. We wish to form the Väisälä frequency based on the external stratification using potential temperature at 900 mb, representative of the temperature maximum layer (Figure 2) and at 850 mb, a standard level, in addition to N_{500}.

$$N_{900} = \left(\frac{g}{\bar{\theta}_{900}} \frac{\Delta\theta_{900}}{h_{900}}\right)^{1/2},$$

$$\bar{\theta}_{900} = (\theta_{900} + \theta_s)/2, \qquad \Delta\theta_{900} = \theta_{900} - \theta_s,$$

$$h_{900} = 67.4\bar{\theta}_{900} \log_{10}(P_s/900), \tag{14}$$

where θ_{900} is the potential temperature at 900 mb and P_s is surface pressure. N_{850} is defined in an analogous manner. The correlation of Cg and α with N', N_{500}, N_{900} and N_{850} are given in Table 5. Nine values have been excluded from the analysis with $Cg > 0.06$, $\alpha < 0$ and $\alpha > 60$. The Cg correlation with N_{900} is $R = 0.39$ and α is $R = 0.30$; plots of Cg and α as a function of N_{900} are shown in Figs. 9 and 10. We note that much of the variability is compressed for values greater than the median, $\bar{N}_{900} = 0.024\ \mathrm{s}^{-1}$. This suggests a power law transformation. The variation of Cg and α with Z_* from modeling studies (Fig. 3) also suggests a power law dependence. The correlation of Cg increases to $R = 0.41$ with a fourth power dependence and remains constant for α for a quadratic dependence (Figs. 11 and 12) giving

$$Cg = 0.037 - 8.3 \times 10^{-3} \left(\frac{N_{900}}{\bar{N}_{900}}\right)^4,$$

$$\bar{N}_{900} = 0.024\ \mathrm{s}^{-1}, \tag{15}$$

$$\alpha = 11.7 + 13.1 \left(\frac{N_{900}}{\bar{N}_{900}}\right)^2. \tag{16}$$

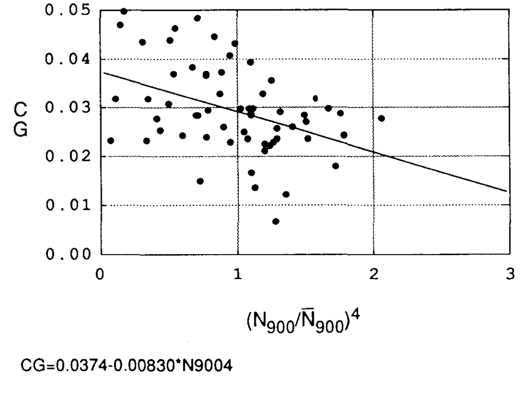

Fig. 11. Plot of Cg versus $(N_{900}/\bar{N}_{900})^4$. The regression curve (15) is shown.

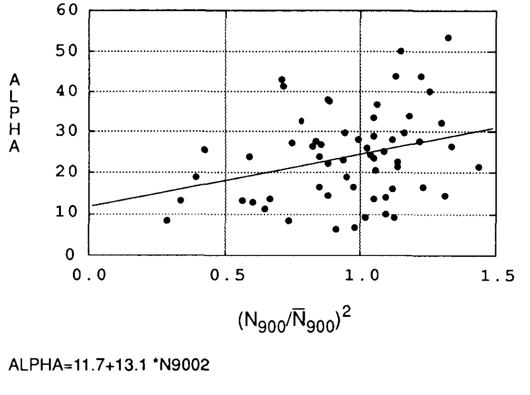

Fig. 12. Plot of α versus $(N_{900}/\bar{N}_{900})^2$. The regression curve (16) is shown.

This makes the turning angle linear in the temperature difference $\Delta\theta_{900}$ and Cg quadratic in $\Delta\theta_{900}$. The expanded variance for Cg is 17%. Note that the dependency in (15) and (16) does not include a velocity scale as in bulk Richardson number similarity formulations (Yamada, 1976)

$$R_B = \frac{h^2 N^2}{G^2}. \tag{17}$$

If potential temperature is available only from standard levels (i.e., 850 mb) the following equations are proposed (Figs. 13 and 14)

$$Cg = 0.036 - 6.9 \times 10^{-3} \left(\frac{N_{850}}{\bar{N}_{850}}\right)^5,$$

$$\bar{N}_{850} = 0.022\ \mathrm{s}^{-1}, \tag{18}$$

$$\alpha = 14.7 + 9.6 \left(\frac{N_{850}}{\bar{N}_{850}}\right)^4. \tag{19}$$

The correlation of Cg from (18) is $R = 0.33$ and for α is 0.31; 11% of the variance is explained. We note from Fig. 2 that the 850 mb level is above or near the top of the temperature maximum layer and thus (18) is subject to more scatter than (15). N_{500} is not as good a predictor of Cg as either N_{900} or N_{850} with an $R = 0.17$. We propose that an external stability parameter for the boundary layer, best represented by N_{900}, is a good indicator of the influence of stratification on external boundary layer parameters such as Cg and α. We reason that because most of the ABL above the surface layer is near a critical Richardson number of 0.25 (Walter and Overland, 1991), the total amount of shear that can be maintained in the boundary layer, and thus the reduction in Cg, is given by the external temperature difference. The detailed internal structure of shear and stratification is of less importance to values of Cg and α. This suggests why the stratification just above the inversion base was not as good a predictor as an external stability measure.

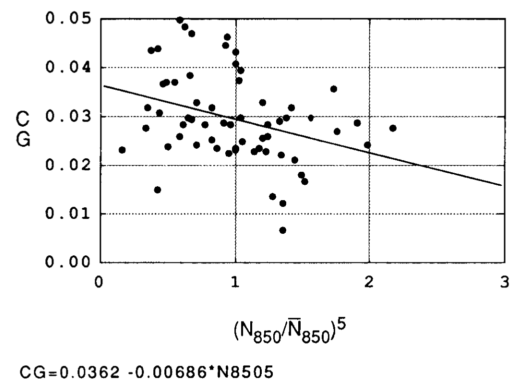

Fig. 13. Plot of Cg versus $(N_{850}/\bar{N}_{850})^5$. The regression curve (18) is shown.

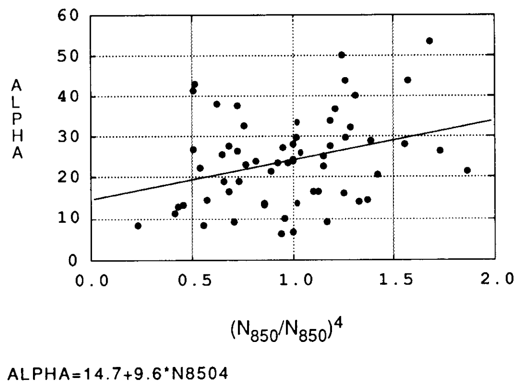

Fig. 14. Plot of α versus $(N_{850}/\bar{N}_{850})^4$. The regression curve (19) is shown.

As a final comparison we use (15) and (18) to estimate Cg for the CEAREX oceanography camp case (Walter and Overland, 1991). The observed Cg values were calculated from direct flux measurements made by an instrumented aircraft. Observed values were 0.014 for 27 March 1989 and 0.015 for 30 March 1989. These are extremely low values, possibly the lowest observed, and are well below the lower hinge for the CEAREX ship drift of 0.023. Formula (15) gives a value of $Cg = 0.011$ for 27 March and 0.014 for 30 March. Formula (18) gives a value of $Cg = 0.015$ for 27 March and 0.014 for 30 March. Thus we have some confidence in (15) and (18) for cases away from the median case for the CEAREX drift.

6. Variation in regional roughness

Cg increases for rough ice typical of small floes in first-year sea ice or the marginal ice zone. Observations for the winter Bering Sea from aircraft-based direct-flux measurements are $Cg = 0.024, 0.035, 0.047$ (Overland, 1985).

For regional seas with roughness different from the central Arctic we propose:

$$Cg = 0.028\left(\frac{C_D}{C_{Do}}\right)^{0.2}, \quad \alpha = 25°,$$

$$C_{Do} = 2.5 \times 10^{-3} \quad \text{stable conditions} \tag{20}$$

$$Cg = 0.034\left(\frac{C_D}{C'_{Do}}\right)^{0.3}, \quad \alpha = 15°,$$

$$C'_{Do} = 3.0 \times 10^{-3} \quad \text{near-neutral conditions.} \tag{21}$$

C_D is the 10 m neutral drag coefficient (Table 6) after Guest and Davidson (1987). For a constant geostrophic wind the 10 m measured wind will decrease as surface roughness increases; if the wind speed at 10 m in (7) did not change with roughness, the exponents in (20) and (21) would be 0.5 instead of 0.2 and 0.3. The exponents 0.2 and 0.3 were determined from the turbulent closure model which produced Fig. 3 (Overland, 1985). Note that Cg is less sensitive to surface roughness for the stable ABL. To simultaneously account for roughness and stability, the coefficient 0.028 in (20) can be replaced by (15) or (18) and α can be replaced by (16) or (19).

Table 6. *Typical neutral 10-m drag coefficients based on floe roughness and concentration (after Guest and Davidson, 1987)*

Upwind ice concentration	Ice characteristics	$C_D \times 10^3$
Open ocean		1.2–2.1[1]
Ice visible (downwind)		1.6 ± 1.0
1%–5%	type C	2.2 ± 0.4
10%–35%	type A	1.7 ± 0.3
	type B	2.1 ± 0.3
	type C	2.7 ± 0.4
40%–65%	type A	1.9 ± 0.3
	type B	2.3 ± 0.4
	type C	3.2 ± 0.6
70%–90%	type A	2.2 ± 0.7
	type B	3.2 ± 0.7
	type C	4.2 ± 0.7
90%–100%	smooth ice[2]	1.5
	arctic pack[2]	2.5
	type C[2]	3.8 ± 1.3

Type A (smooth): floes greater than 100 m which are visually smooth or with gently rolling hummocks.

Type B (rough): 10–100 m floes with 1–2 m ridges spaced 5–50 m apart, some rafting.

Type C (very rough): floe size generally less than 10 m. Floes are irregularly shaped and are heavily rafted, often near the marginal ice zone.

[1] From Large and Pond (1981).

[2] From Overland (1985).

7. Conclusions

The geostrophic drag coefficient and turning angle were calculated from an array of 6 ARGOS drifting buoys centered on measurements from a drifting vessel during October–December 1988 in a region northeast of Svalbard during CEAREX. Ice conditions and meteorological conditions were typical of winter season (October–May) east-central Arctic. Because the data set consisted of values made over 35 days when ice conditions were not changing, the data allowed us to investigate the variability of the geostrophic drag coefficient with stability. Surface air temperature or cloud amount alone are not good predictors of arctic ABL stratification but the difference between θ_{900} or θ_{850}, representative of the temperature maximum layer, and θ_s provide a good measure. The importance of the upper level temperature at 81°N confirms the conclusions of Nakamura and Oort (1988) and Overland and Guest (1991) of the importance of advection of warm air into the Polar Basin in determining the vertical structure of the arctic atmosphere. The importance of inversions formed by lateral advection was earlier noted by Vowinckel and Orvig (1970).

The median and variability of Cg and α in the CEAREX data set are consistent with regional values from AIDJEX. Thorndike and Colony (1982) also note little evidence of geographic variability in ice speed-geostrophic wind ratios. Thus to zero order a Cg of 0.028 and α of 25° is recommended for use in sea ice models of the central Arctic during October through May. Use of the gradient wind (Appendix) is preferred to the geostrophic wind with these relations so that surface wind stress will not be overestimated in small cyclonic storm systems. If information is available on θ_{900} or θ_{850} and θ_s, a stability correction can be made based on (15–19). This correction provides a 17% improvement in Cg values based on reduction in variance. It would be instructive to see if θ_{900} values can be calculated sufficiently from

TOVS temperature soundings obtained from satellites to provide basin-wide stability corrections. Potential temperature at 850 mb can be used for stability corrections and is available from routine atmospheric analyses.

Acknowledgments

We thank Peter Guest and Nick Bond for discussions on the data analyses of the CEAREX data set. Peter Guest, Keith Jones, Gary Lackmann, and Oeystein Skagseth collected the data at the *Polarbjorn* site. Sigrid Salo conducted the buoy deployment.

10. Appendix

The gradient wind, G_{grad}, can be solved iteratively from the geostrophic wind G_{geo}

$$G^{n+1}_{\mathrm{grad}} = (1 - kG^{n}_{\mathrm{grad}})\, G_{\mathrm{geo}}, \tag{A1}$$

with $G^{1}_{\mathrm{grad}} = G_{\mathrm{geo}}$ (Endlich, 1961). The curvature k is calculated from a second-order finite difference approximation to

$$k = (P_x^2 + P_y^2)^{-2} \times (P_y^2 P_{xx} - 2P_x P_y P_{xy} + P_x^2 P_{yy}), \tag{A2}$$

where x and y represent east and north differentiation of the sea level pressure field, P.

REFERENCES

Brown, R. A. 1981. Modeling the geostrophic drag coefficient for AIDJEX. *J. Geophys. Res. 86*, 1989–1994.

Carsey, F. and Leavitt, E. 1977. Pibal/acoustic radar data in measurement and computation of air stress over pack ice. *AIDJEX Bull. 36*, 87–128.

CEAREX Drift Group. 1990. CEAREX Drift Experiment. *Eos Trans. AGU 71*, 1115–1118.

Danard, M. 1988. A diagnostic method for computing the surface wind from the geostrophic wind including the effects of baroclinity. *Mon. Weather Rev. 116*, 2712–2716.

Endlich, R. M. 1961. Computation and uses of gradient winds. *Mon. Weather Rev. 89*, 187–191.

Fiedler, F. and Panofsky, H. A. 1972. The geostrophic drag coefficient and the effective roughness length. *Q.J.R. Meteorol. Soc. 98*, 213–220.

Guest, P. S. and Davidson, K. L. 1987. The effect of observed ice conditions on the drag coefficient in the summer East Greenland Sea marginal ice zone. *J. Geophys. Res. 92*, 6943–6954.

Hibler, W. D. III and Walsh, J. E. 1982. On modeling seasonal and interannual fluctuations of arctic sea ice. *J. Phys. Oceanogr. 12*, 1514–1523.

Joffre, S. M. 1983. Determining the form-drag contribution to the total stress of the atmospheric flow over ridged sea ice. *J. Geophys. Res. 88*, 4524–4530.

Katz, D. I. 1979. *An investigation of the arctic planetary boundary layer.* MS Thesis, Univ. of Wash., Seattle, WA, 160 pp.

Kitaigorodskii, S. A. 1988. A note on similarity theory for atmospheric boundary layers in the presence of background stable stratification. *Tellus 40A*, 434–438.

Kitaigorodskii, S. A. and Joffre, S. M. 1988. Simple scaling for the height of the stratified atmospheric boundary layer. *Tellus 40A*, 419–433.

Large, W. G. and Pond, S. 1981. Open ocean momentum flux measurements in moderate to strong winds. *J. Phys. Oceanogr. 11*, 342–336.

Nakamura, N. and Oort, A. H. 1988. Atmospheric heat budgets of the polar regions. *J. Geophys. Res. 93*, 9510–9524.

Overland, J. E. 1985. Atmospheric boundary layer structure and drag coefficients over sea ice. *J. Geophys. Res. 90*, 9029–9049.

Overland, J. E. and Guest, P. S. 1991. Control of minimum snow and air temperatures over arctic sea ice during winter. *J. Geophys. Res. 96*, 4651–4662.

Overland, J. E., Mobley, C. D. and Brown, R. A. 1980. METLIB-A program library for calculating and plotting marine boundary layer winds. *NOAA Tech. Memo. ERL PMEL-20*, 82 pp., Seattle, Wash., available as PB81-141038, Natl. Tech. Inf. Serv., Springfield, Va.

Preller, R. H. and Posey, P. G. 1989. The polar ice prediction system, a sea ice forecasting system. NORDA Report 212, Naval Ocean Research and Development Activity, Stennis Space Science Center, MS, 42 pp.

Serreze, M. C. and Barry, R. G. 1988. Synoptic activity in the Arctic Basin. *J. Climate 1*, 1276–1295.

Snedecor, G. W. and Cochran, W. G. 1989. *Statistical methods.* Iowa State University Press, Ames, Iowa, 136–137.

Sverdrup, H. U. 1933. *The Norwegian North Polar Expedition with the "Maud"*, vol. II, Meteorology. Geophysical Institute, Bergen, Norway, 331 pp.

Thorndike, A. S. and Colony, R. 1982. Sea ice motion in response to geostrophic winds. *J. Geophys. Res. 87*, 5845–5852.

Vowinckel, E. and Orvig, S. 1970. Climate of the North Polar Basin. In: *Climate of the polar regions*, S. Orvig, editor, Elsevier Science Publishing, New York, 129–252.

Walter, B. A. and Overland, J. E. 1991. Aircraft observations of the mean and turbulent structure of the atmospheric boundary layer during spring in the central Arctic. *J. Geophys. Res. 96*, 4663–4674.

Walter, B. A., Overland, J. E. and Gilmer, R. O. 1984. Air-ice drag coefficients for first-year sea ice derived from aircraft measurements. *J. Geophys. Res. 89*, 3550–3560.

Yamada, T. 1976. On the similarity functions A, B, and C of the planetary boundary layer. *J. Atmos. Sci. 33*, 781–793.